

## A comparison of mean density and microscale density fluctuations in a CME at $10 R_{\odot}$

B. J. Lynch<sup>1</sup> and W. A. Coles

Department of Electrical and Computer Engineering, University of California, San Diego, La Jolla, CA, USA

N. R. Sheeley Jr.

E. O. Hulburt Center for Space Research, Naval Research Laboratory, Washington, DC, USA

Received 29 September 2001; revised 7 March 2002; accepted 12 March 2002; published 5 October 2002

[1] We have observed intensity scintillation (IPS) of the radio source 0854 + 201 at 8 GHz on August 2, 2000 during the passage of a coronal mass ejection (CME) across the line of sight. The source was at a distance of  $10 R_{\odot}$  over the north solar pole. Simultaneous observations with the LASCO C3 instrument allow us to model the mean density  $N_e$  and the microscale density fluctuations  $\delta N_e$  within the CME. We find that  $N_e$  increased by a factor of 2.18 but  $\delta N_e$  increased by only 1.76, so the ratio  $\delta N_e/N_e$  is 19% smaller than in the pre-CME slow wind. During the passage of the CME a short burst of enhanced turbulence doubled the IPS variance but was not visible in the C3 images. This was likely caused by a thin flux tube crossing the line of sight. Detailed modeling indicates that the diameter of the tube was 41,000 km and its density was 14.5 times the CME density. *INDEX TERMS:*

7513 Solar Physics, Astrophysics, and Astronomy: Coronal mass ejections; 2164 Interplanetary Physics: Solar wind plasma; 2111 Interplanetary Physics: Ejecta, driver gases, and magnetic clouds.

**Citation:** Lynch, B. J., W. A. Coles, and N. R. Sheeley Jr., A comparison of mean density and microscale density fluctuations in a CME at  $10 R_{\odot}$ , *Geophys. Res. Lett.*, 29(19), 1913, doi:10.1029/2001GL014152, 2002.

### 1. Observations

[2] Intensity scintillation at 8 GHz is “weak” at  $10 R_{\odot}$ , so it provides a linear measure of the density fluctuations with spatial scales of the order of 50 km. With the LASCO C3 instrument [Brueckner *et al.*, 1995] it is possible to make a direct comparison between these “microscale” fluctuations and the mean density. Both observations involve line of sight integrals which cannot be directly inverted, but a useful comparison can be made by fitting a simple CME model to the two data sets simultaneously. The comparison can be made with respect to the pre-CME slow wind without requiring absolute calibration of the IPS or the coronagraph.

[3] The structure of the CME is shown clearly in Figure 1. This is a grey-scale version of the summary images available on the SOHO web site (<http://sohowww.nascom.nasa.gov/>). A description of the image processing is available on the LASCO web site ([http://lasco-www.nrl.navy.mil/idl\\_pros/help\\_synoptic.html](http://lasco-www.nrl.navy.mil/idl_pros/help_synoptic.html)).

[4] Eight C3 images taken during the passage of the CME are shown with the same processing in Figure 2. A 3-hour average of the pre-event corona is used as the slow wind background reference. These images were used to estimate the CME velocity using the running difference technique described by Sheeley *et al.* [1997]. Height-time plots at the position angle of the radio source show that the velocity of the leading edge was  $546 \pm 26$  km/s and the velocity in the center of the CME was  $444 \pm 21$  km/s. As the CME is relatively fast, one might expect to see some compression at the leading edge.

[5] To obtain an estimate of the integrated mean electron density from the C3 images, we must separate the K (electron) component from the F (dust) component. This is done using polarization measurements because the polarization of the K and F components are very different. We assume that the F component is independent of the CME and calculate it from the pre-CME reference. We know  $P_F/B_F = 0.002$  at  $10 R_{\odot}$  [Mann, 1992]. We calculated  $P_K/B_K$  using well-known expressions [van de Hulst, 1950; Billings, 1966; Hayes *et al.*, 2001]. At  $10 R_{\odot}$  the familiar coronal density models are not valid, so we used two spherically symmetric solar wind density models: a polar coronal hole model [Guhathakurta *et al.*, 1999]; and an equatorial streamer model [Muhleman and Anderson, 1981]. The two models yielded values of  $P_K/B_K = 0.507$  and  $0.5164$ , confirming that the polarization is not very sensitive to the density. We measured  $P_T = P_F + P_K$  and  $B_T = B_F + B_K$  at the pre-CME reference location by averaging 17 pixels around the IPS location on the polarized images from August 1 and 2. We obtained  $P_T/B_T = 0.0553 \pm 0.0043$ . Thus  $B_{KREF} = 0.105 B_T$  and  $B_{FREF} = 0.895 B_T$ . We then obtain the K corona brightness  $B_K(t)$  during the passage of the CME from the observed total brightness  $B_T(t)$  at the IPS location, using  $B_K(t) = B_T(t) - B_{FREF}$ . The normalized brightness  $B_K(t)/B_{KREF}$  is plotted in the top panel of Figure 3.

[6] The IPS measurements were made using three antennas of the VLBA at Kitt Peak, Pietown, and Los Alamos. The data were sampled at 100 Hz and spectra were analyzed in 10 minute blocks. The low frequency drift was removed with a 0.2 Hz highpass filter and the receiver noise was estimated and subtracted. The intensity variance  $\delta I^2$  was computed by integrating under the autospectra. The variance was normalized by the pre-CME value and plotted in the bottom panel of Figure 3. The CME is very well defined on this plot. Just after the peak of the CME a large but short-lived increase occurred. The data were reanalyzed in 2 minute blocks to provide better resolution of this burst.

<sup>1</sup>Now at Department of Atmospheric, Oceanic, and Space Sciences, University of Michigan, Ann Arbor, USA.

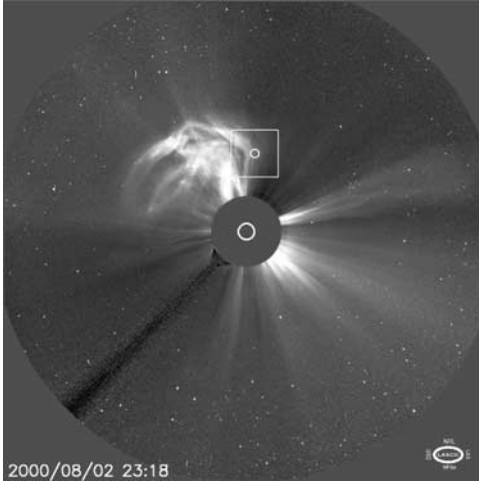


**Figure 1.** A LASCO C3 image of the CME during our IPS observation. The location of 0854 + 201 is circled. The square marks the  $100 \times 100$  pixel region expanded in Figure 2.

The burst cannot be due to radio interference because it was observed at two antennas which are 200 km apart (the Kitt Peak antenna was temporarily stowed due to high wind).

## 2. Modeling

[7] We write the line of sight integrals in terms of  $\theta$ , the angle subtended at the sun, which is a more convenient form for numerical integration through an inhomogeneous medium. The IPS variance depends on many factors which are distance dependent. These are discussed, for example, by *Coles et al.* [1995]. However the elongation  $x$  of the radio source was essentially constant during the CME passage, so we can simplify the line of sight integral (over  $z = r \sin(\theta)$ ) for the intensity variance to

$$\begin{aligned} \delta I^2(x) &= K \int_{-1}^{\infty} \delta N_e^2(r) \sqrt{1+z} dz \\ &= K \int_{-\pi/2 + \sin^{-1}(x)}^{\pi/2} \delta N_e^2(\theta) \frac{\sqrt{1+x \tan \theta}}{\cos^2 \theta} d\theta. \end{aligned} \quad (1)$$

Here  $x = r \cos(\theta)$  is the distance of closest approach and  $K$  is a constant which will be normalized out. The variance depends on the square root of the distance from the Earth, (here =  $1 + z$ ).

[8] We model the body of the CME as an oblate spheroid ball of uniform density to match the image shown in Figure 1. The measured angular width is  $84.4 \pm 3.0$  deg at  $10 R_{\odot}$ , and the time for the CME to pass  $10 R_{\odot}$  was  $234 \pm 22$  min. Using a velocity of 500 km/s we estimate the apparent axial ratio is  $1.46 \pm 0.15$ . If it were exactly an oblate spheroid the true axial ratio would be 1.57, but the difference is within the statistical error and we don't know the shape well enough to justify further refinement. The normalized mean and rms density ( $N_e$  and  $\delta N_e$ ), and the duration at the IPS location are the only free parameters. The data weights were adjusted so both data sets contribute equally to the mean squared error. The model best-fit to the data, excluding the IPS data

between 23:30 and 23:40 UT, gives:  $N_e = 2.18$ ,  $\delta N_e = 1.76$ , duration = 170 min. This model is plotted over the observations on Figure 3. The model matches the leading edge of the CME in both observations reasonably well. However at the trailing edge we see that the IPS falls more quickly than the C3 brightness. This suggests that the trailing edge of the CME is less turbulent, but the effect is marginally significant. The ratio  $\delta N_e / N_e$ , which we define to be unity in the pre-CME slow wind, is slightly lower in the CME,  $\delta N_e / N_e = 0.81 \pm 0.10$ , which is also marginally significant.

[9] The transient IPS enhancement between 23:30 and 23:40 UT is not visible in the C3 images but we can make some inferences about its structure. We tried to fit it with a simple model of a spherical plasmoid with the same velocity as the CME itself. The duration of the IPS response implies a diameter of  $253,000 \pm 32,000$  km and the magnitude of the IPS increase implies a density of  $12.8 \pm 2.5$  times the background. Although this model fits the IPS data very well, it would increase the C3 brightness by 13.5% over a region 7 pixels in diameter. This is a  $1 \sigma$  increase in

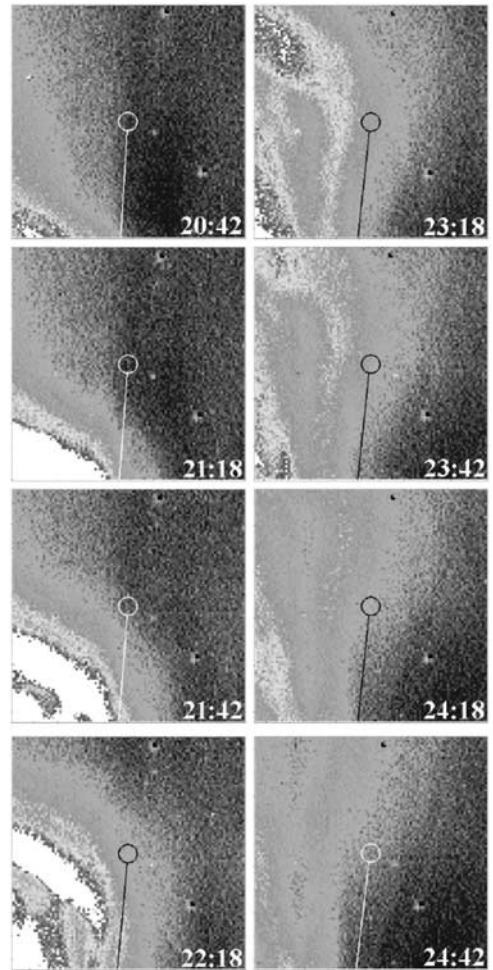


**Figure 2.** Expanded C3 images showing the passage of the CME across the IPS line of sight. Each panel has undergone the same background subtraction as Figure 1, but the contrast was adjusted individually to enhance the CME structure. The IPS source is circled. A line drawn from the circle towards the center of the sun indicates the radial direction. The time (UT) is indicated on each frame.

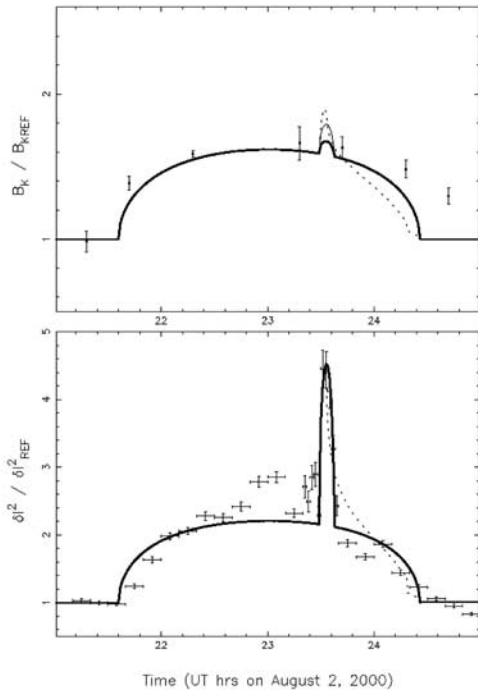


**Figure 3.** *Top*, brightness of the K corona at the IPS location normalized by the pre-CME value. *Bottom*, IPS intensity variance normalized by the pre-CME value. The best-fit shell (dotted), plasmoid (thin solid), and flux tube (thick solid) models are drawn over the data. The plasmoid and flux tube models have identical IPS profiles. The error bars do not include normalizing errors common to all points. These are 8% for the brightness and 2% for the intensity variance.

brightness over the plasmoid and would normally have been visible in the C3 image. We simulated this enhancement and found that it was detectable in a single image 75% of the time. Since it would have been visible in at least two images, and we know exactly where it would be, it is unlikely that such a compact plasmoid can be present. An alternative model is that the enhancement is caused by a thin radially-extended structure which is pushed laterally across the line of sight as the CME passes. It could be either a thin shell or a thin flux tube. We have tested both models using a transverse velocity calculated from the images in Figure 2.

[10] At the time of the IPS enhancement the radio source was near the edge of the CME in a region with a steep transverse density gradient. We measured the position of a constant brightness contour in successive images at 23:18 and 23:42 UT. To reduce the estimation error we chose a contour with a steep gradient, and we smoothed the images over 9 pixels. The apparent velocity of this contour line,  $80.5 \pm 15.7$  km/s, provides an estimate of the transverse velocity of the plasma if the mean CME density at  $10 R_{\odot}$  is constant.

[11] We model the flux tube as a simple addition to the bulk CME. For the shell we use the radius of curvature of the bulk CME and fill the inside with the pre-CME density level. If the inside of the shell is filled with the bulk CME density the model cannot be fit at all. The best-fit flux tube, plasmoid, and shell models are plotted over the observations

on Figure 3 as thick solid, thin solid, and dotted lines respectively. The flux tube and plasmoid models fit the IPS equally well and are indistinguishable on this plot. However the flux tube provides a smaller enhancement in the C3 brightness,  $0.5 \sigma$ . The IPS response of the shell is more extended than either the plasmoid or flux tube models, therefore the best fit shell is thinner than either. The shell model predicts an enhancement of  $2 \sigma$  in the C3 brightness, and it does not fit either data set as well as the plasmoid or flux tube models. The minimum  $\chi^2(34)$  values for the flux tube and shell models are 62.2 and 94.9 respectively. A flux tube or a shell would appear in a C3 image as a radial line, one pixel wide and many pixels long. Simulations showed that a one pixel wide linear feature becomes distinguishable from the background noise with a brightness enhancement of between 1 and  $1.5 \sigma$ . Thus the shell would have been easily detectable in the C3 image, whereas the flux tube would be lost in the background noise.

[12] The flux tube diameter is  $40,800 \pm 7,900$  km and its density is  $31.5 \pm 6.2$  times the reference background. The most straightforward interpretation of this model is that the flux tube was pre-existing and was pushed aside by the CME. In this case one has to explain a rather thin dense structure at  $10 R_{\odot}$ .

### 3. CME Complexity in IPS

[13] The objective of the IPS measurements had been to estimate the flow velocity of the quasi-static wind. The auto- and cross-correlations between the antennas were calculated so time delays could be measured and the velocity distribution estimated [Grall *et al.*, 1996]. The

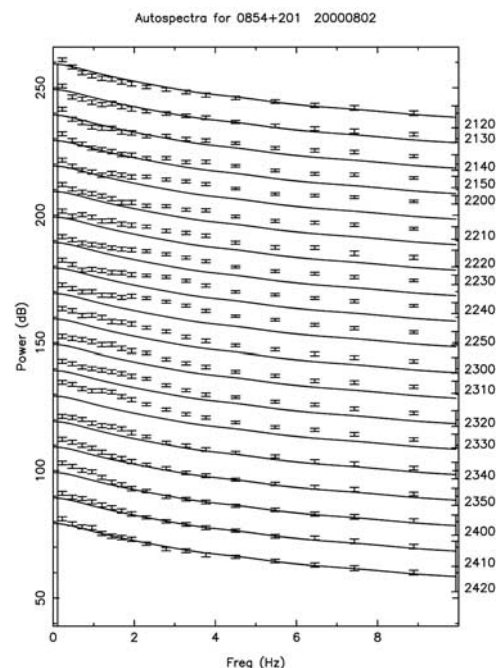


**Figure 4.** The IPS auto-spectra estimated at 10-minute intervals during the passage of the CME. The time (UT) is indicated to the right of each. The error bars indicate the data, the solid lines are a pre-CME slow wind model drawn over each spectrum for comparison.

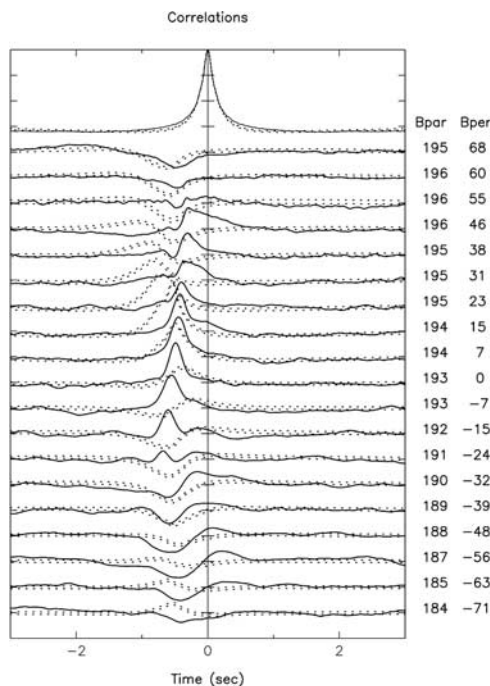


**Figure 5.** The IPS auto- and cross-correlations corresponding to the spectra of Figure 4. The top trace is the auto-correlation. The cross-correlations are offset by 0.33 each. The parallel and perpendicular components of the interantenna baseline are given in km. The solid lines are the data, the dotted lines are a pre-event slow wind model shown for comparison.

spectra and correlations show a complex behavior during the CME passage, which can be explained using our model, but which is too complex to derive a velocity independent of C3 observations.

[14] The IPS auto-spectra, taken on 10 minute intervals, are shown in Figure 4. The CME first appears as a high frequency enhancement. This is because it enters the IPS line of sight with the magnetic field almost perpendicular to the radial flow direction (as seen in Figure 2 at 21:42). The spatial scale is much smaller in this direction, so it creates a high frequency enhancement. As the CME passes the magnetic field rotates until it is almost aligned with the flow. The spectral enhancement moves to lower frequencies and finally disappears. The burst of increased scintillation at 23:30 UT does not change the shape of the spectrum, but increases the amplitude overall. If one used the width of the spectrum as a measure of the velocity as do *Manoharan and Ananthakrishnan* [1990], then one would interpret this variation in spectral width as a velocity change. In fact all the variation is actually caused by change in the apparent spatial scale due to the changing angle between the highly anisotropic structure and the velocity vector.

[15] The time varying nature of the CME is also evident in the cross-correlation functions shown in Figure 5. The CME enters the line of sight as a narrow positive bump in the cross-correlation. As the CME passes this bump moves to larger time lags and becomes broader before finally disappearing. In the quasi-static solar wind such cross-

correlations can be used to estimate the axial ratio, the spectral exponent, and the velocity distribution of the microstructure. However this requires the spatial structure and velocity be quasi-static and that is clearly not valid during this CME. One suspects that it is never valid during a CME, although the problem is less severe outside of  $20 R_{\odot}$  where the microstructure is more isotropic. In this case we can fit all the cross-correlation functions individually but we must use a different angle between the magnetic field and the flow for each correlation.

#### 4. Conclusion

[16] A fast CME is easily seen in IPS at  $10 R_{\odot}$ , and can be modeled in conjunction with simultaneous coronagraph images. These indicate that  $\delta N_e/N_e$  in the CME slightly lower than in the background slow wind. In general IPS is more sensitive to small, but dense, structures than is a coronagraph because it responds to  $N_e^2$  rather than  $N_e$ . In this CME the IPS shows a structure 30 times denser than the background which is so thin that it is not visible in the C3 coronagraph. Finally we see that the spatial structure of this CME was far too complex to unravel with IPS alone.

[17] **Acknowledgments.** This work was supported by the National Science Foundation under grant ATM-9627228 and the Office of Naval Research under the Solar Magnetism and the Earth's Environment 6.1 Accelerated Research Initiative. One of the authors (BJL) was partially supported by a grant from the IEEE Antennas and Propagation Society, and a Chancellor's Undergraduate Scholarship from UCSD. The authors would like to thank R. A. Howard for help with the LASCO brightness analysis.

#### References

- Billings, D. E., *A Guide to the Solar Corona*, New York, Academic Press, 1966.
- Brueckner, G. E., et al., The Large Angle Spectroscopic Coronagraph (LASCO), *Solar Phys.*, *162*, 357, 1995.
- Coles, W. A., R. R. Grall, M. T. Klinglesmith, and G. Bourgois, Solar cycle changes in the level of compressive microturbulence near the sun, *J. Geophys. Res.*, *100*, 17,069, 1995.
- Grall, R. R., W. A. Coles, M. T. Klinglesmith, A. R. Breen, P. J. S. Williams, and R. Esser, Rapid acceleration of the polar solar wind, *Nature*, *379*, 429, 1996.
- Guhathakurta, M., A. Fludra, S. E. Gibson, D. Biesecker, and R. Fisher, Physical properties of a coronal hole from coronal diagnostic spectrometer, Mauna Loa coronagraph, and LASCO observations during the whole sun month, *J. Geophys. Res.*, *104*, 9801, 1999.
- Hayes, A. P., A. Vourlidas, and R. A. Howard, Deriving the electron density of the solar corona from the inversion of total brightness measurements, *Astrophys. J.*, *548*, 1081, 2001.
- Mann, I., The solar F-corona: Calculations of the optical and infrared brightness of the circumsolar dust, *Astron. & Astrophys.*, *261*, 329, 1992.
- Manoharan, P. K., and S. Ananthakrishnan, Determination of solar wind velocities using single station measurements of interplanetary scintillations, *Mon. Not. R. Astron. Soc.*, *244*, 691, 1990.
- Muhleman, D. O., and J. D. Anderson, Solar wind electron densities from Viking dual-frequency radio measurements, *Astrophys. J.*, *247*, 1093, 1981.
- Sheeley, N. R., Jr., et al., Measurements of flow speeds in the corona between 2 and 30 Rs, *Astrophys. J.*, *484*, 472, 1997.
- van de Hulst, H. C., Electron density of the solar corona, *Bull. Astron. Inst. Neth.*, *11*, 135, 1950.

W. A. Coles and B. J. Lynch, Department of Electrical and Computer Engineering, Mail Code 0407, University of California, San Diego La Jolla, CA 92092-0407, USA. (coles@ece.ucsd.edu; blynch@ece.ucsd.edu)

N. R. Sheeley Jr., E. O. Hulburt Center for Space Research, Naval Research Laboratory, Washington, DC 20375-5352, USA.